JOURNAL OF MAGNETIC RESONANCE 20, 214–231 (1975)

Pure Nuclear Quadrupole Resonance Studies of Structural Phase Transitions

ROBIN L. ARMSTRONG

Department of Physics, University of Toronto, Toronto, Canada, M5S 1A7

Presented at the Third International Symposium on
Nuclear Quadrupole Resonance, Tampa, Florida, April, 1975

Structural phase transitions of the tilting variety occur and transform certain cubic antifluorite and cubic perovskite structures to lower symmetry structures. This article provides a review of recent advances in our understanding of these phase transitions as revealed by pure nuclear quadrupole resonance (NQR) experiments in K_2PtBr_6, K_2ReCl_6, $CsPbCl_3$, and K_2OsCl_6. In general, the results show that both NQR frequency and spin-lattice relaxation data may be analyzed to reveal the condensation of the rotary-lattice mode responsible for a particular transition. The similarity of the antifluorite and perovskite structures with respect to tilting type phase transitions is illustrated both by the behavior of the NQR data and by the results of rigid-ion model calculations. In particular, the K_2PtBr_6 data provide experimental confirmation of the dominance of the anharmonic Raman process as a relaxation mechanism for the bromine nuclei. The K_2ReCl_6 data provide an example for analysis in which the temperature dependence of the NQR frequency data is dominated by specific volume effects. The $CsPbCl_3$ relaxation data reflect the extraordinary degree of anharmonicity present in the cubic phase. The substance K_2OsCl_6 provides evidence for the formation of tetragonal phase dynamic clusters in the cubic phase. In all instances the interpretation makes use of available information from other types of experiments. For example, the NQR frequency spectrum of $CsPbCl_3$ is shown to be consistent with structural determinations from neutron scattering studies.

1. INTRODUCTION

The cubic antifluorite (R_2MX_6) and cubic perovskite (RMX_3) structures are very similar; both are describable in terms of a framework of MX_6 octahedra with the R ions occupying interstitial sites. In a certain sense the cubic antifluorite structure is equivalent to a half empty perovskite structure. These structures are illustrated in Fig. 1. Many crystals possessing these structures at high temperatures undergo purely displacive phase transitions of the tilting variety at lower temperatures. For such a transition the equilibrium orientation of the MX_6 octahedra may be taken as the primary order parameter η. In the high temperature phase the principal axes of the octahedra in their equilibrium orientations are parallel to the cubic axes of the Bravais lattice and $\eta = 0$. In the low temperature phase the principal axes of the octahedra reorient through an angle θ which is some function of the temperature and $\eta = \theta(T)$. The distorted RMX_3 structure is illustrated in Fig. 2. The reorientation of the MX_6 octahedra is accompanied by a small distortion of the lattice.

A purely displacive phase transition is caused by the condensation of a particular normal mode of the phonon in the cubic phase whose eigenvector corresponds to the atomic displacements in the structure stabilized below the transition temperature T_c.

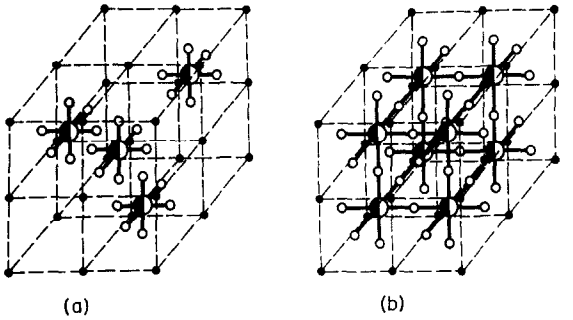

FIG. 1. (a) The cubic antifluorite (R_2MX_6) structure. (b) The cubic perovskite (RMX_3) structure.

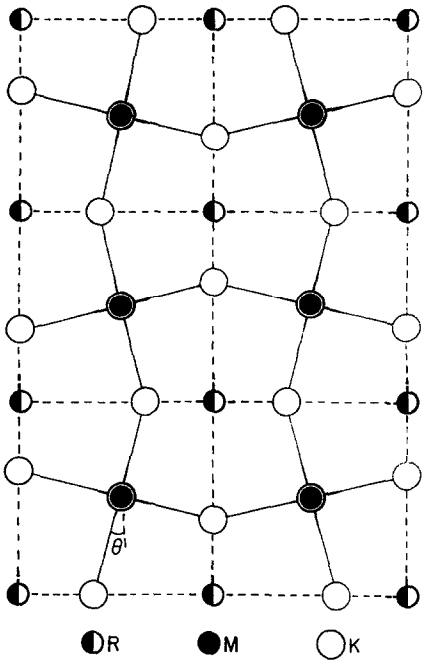

FIG. 2. Orientation of MX_6 octahedra in the tetragonal phase of an RMX_3 structure.

Group theoretical considerations provide the various possible mode candidates. As the temperature is lowered to T_c the frequency of the phonon mode driving the phase transition decreases and at T_c the restoring force for this mode vanishes thereby allowing the atoms to shift to their new equilibrium positions. The identification of the *soft modes* associated with specific transitions is essential to the verification of this dynamical model.

One feature of a purely displacive phase transition that distinguishes it from an order disorder phase transition is the very small specific heat anomaly associated with the transition. The physical reason for such a small change is that the soft mode associated with the transition affects only a very small region of **k**-space, thereby giving rise to very little entropy change in the system.

The intent of this paper is to review the recent progress made towards a better understanding of tilting type phase transitions in R_2MX_6 and RMX_3 structures using the nuclear quadrupole resonance technique.

2. BROMINE NQR IN K_2PtBr_6 (*1*)

The ^{79}Br nuclear quadrupole resonance frequency data obtained from a powder sample of K_2PtBr_6 over the temperature range from 4 to 450 K are shown in Fig. 3. Above 169 K a single resonance line is observed. Just below 169 K two resonance lines

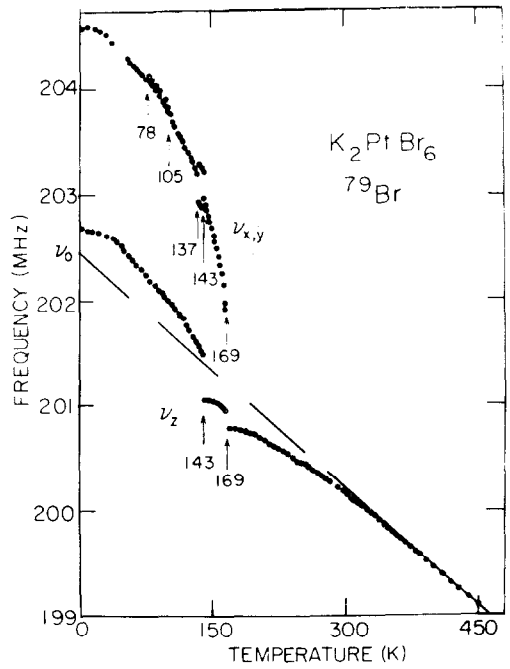

FIG. 3. Temperature dependence of the ^{79}Br NQR frequency in K_2PtBr_6.

are observed; the intensity of the high frequency line is twice that of the low frequency line. This behavior is consistent with a reduction of crystal symmetry from cubic to tetragonal accompanied by a reorientation of the $PtBr_6$ octahedra. It will be assumed that this transition is indeed of the tilting variety. The splitting of the lines in the tetragonal phase increases as the temperature is lowered. A point charge calculation (*2*) of the lattice contribution to the electric field gradient at a Br site shows that the line splitting just above 143 K corresponds to a reorientation of the $PtBr_6$ octahedra through ~7°. Although the phase transition at 169 K is the only one that will be considered in detail, it might be noted from Fig. 3 that other transitions occur at 143, 137, 105, and 78 K.

The temperature dependences of NQR frequencies reflect both pure temperature and pure volume effects (*3*). In order to assess the importance of volume effects it is necessary to measure the pressure dependence of the NQR frequency as a function of temperature. Although these data are not available for K_2PtBr_6, they are available for some other members of the R_2MX_6 family and in those cases it has been noticed that explicit volume effects are important in the cubic phase only when the nucleus of interest is contained within a bond possessing π character. Since the Pt–Br bonds in K_2PtBr_6 have only σ character it is reasonable to associate the entire temperature dependence of the NQR frequency with the thermal averaging of the local electric field gradient by the lattice vibrations.

For the analysis of the data in the cubic phase it is assumed that the electric field gradient at a Br site arises entirely from the charge distribution within the relevant Pt–Br bond. That is, the 5 to 10% contribution from the rest of the lattice is neglected. The NQR frequency is given by (*4*)

$$\nu(T) = \nu_0[1 - \tfrac{3}{2}\langle\theta_x^2(T)\rangle - \tfrac{3}{2}\langle\theta_y^2(T)\rangle],$$

where ν_0 is the static lattice resonance frequency and $\langle\theta_\alpha^2(T)\rangle$ is the αth component of the mean-squared angular displacement of the Pt–Br bond which lies in the z-direction. In this case

$$\langle\theta_\alpha^2(T)\rangle = \frac{\hbar}{2NR^2}\sum_{kj}\left|\frac{e_\alpha(\mathrm{Br}|\mathbf{k}j)}{m_{\mathrm{Br}}^{1/2}} - \frac{e_\alpha(\mathrm{Pt}|\mathbf{k}j)}{m_{\mathrm{Pt}}^{1/2}}\right|^2 x\,\frac{1}{\omega_j(\mathbf{k})}\coth\left(\frac{\hbar\omega_j(\mathbf{k})}{2k_B T}\right)$$

where $e_\alpha(\kappa|\mathbf{k}j)/m_\kappa^{1/2}$ is proportional to the displacement of atom κ in normal mode $(\mathbf{k}j)$ of frequency $\omega_j(\mathbf{k})$, N is the number of molecules per unit volume and R is the Pt–Br bond length. Only those lattice modes which involve bond bending give nonzero contributions to the sum. The contribution to $\langle\theta_\alpha^2(T)\rangle$ due to the internal modes of the $PtBr_6$ octahedra can be evaluated using available infrared and Raman data since to a good approximation these mode frequencies and eigenvectors are independent of the crystalline environment. It represents about 15% of the total. Further, it is assumed that the rotary lattice modes are pure throughout the Brillouin zone and that they are the only lattice modes that contribute to $\langle\theta_\alpha^2(T)\rangle$. This is a reasonable assumption because the rotary mode frequency in K_2PtBr_6 is predicted to lie relatively low ($\sim$30 cm^{-1}). The NQR data can then be analyzed to yield a Brillouin zone averaged rotary mode frequency $\bar{\omega}_v$ by means of the relation

$$\Delta\nu_{\mathrm{rot}} = \frac{3\nu_0 k_B T}{I\bar{\omega}_v^2}$$

where $\Delta\nu_{\mathrm{rot}}$ is the portion of $|\nu - \nu_0|$ not accounted for by the consideration of the internal modes, and I is the moment of inertia of the $PtBr_6$ octahedron. The quantity $\bar{\omega}_v$ is defined as

$$\bar{\omega}_v = \left\{\frac{V_c}{(2\pi)^3}\int_{\mathrm{BZ}}\frac{dk}{\omega_{\mathrm{rot}}^2(\mathbf{k})}\right\}^{-1/2}$$

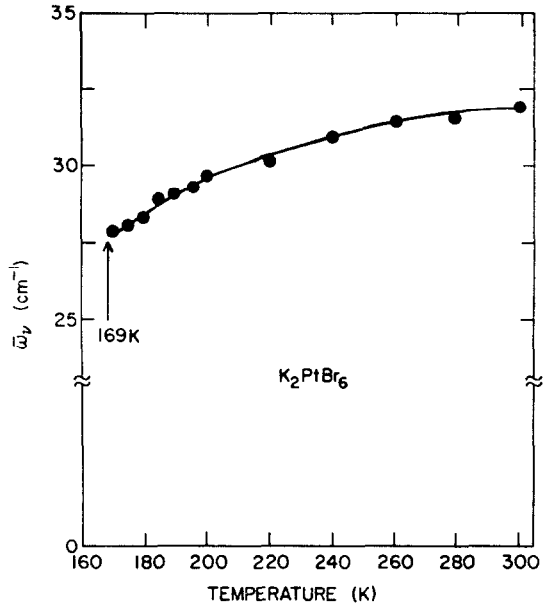

FIG. 4. Temperature dependence of the average rotary-lattice mode frequency $\bar{\omega}_v$.

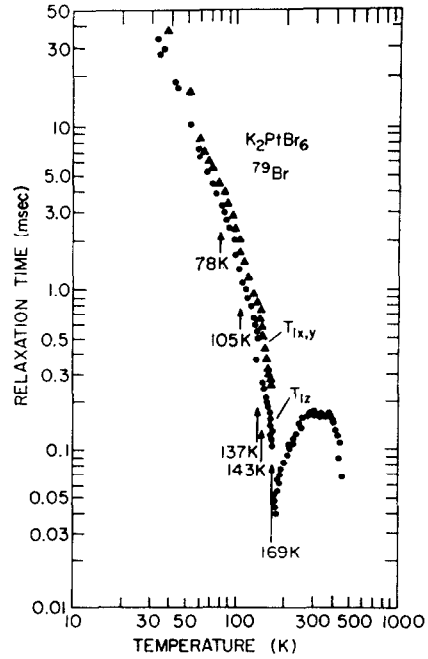

FIG. 5. Temperature dependence of the ^{79}Br spin-lattice relaxation time in K_2PtBr_6.

where V_c is the volume of the unit cell in the direct lattice and the integration is taken over the Brillouin zone. The temperature dependence of $\bar{\omega}_v$ as deduced from the data shown in Fig. 3 is presented in Fig. 4. At 300 K $\bar{\omega}_v \simeq 32$ cm^{-1} whereas at 169 K $\bar{\omega}_v \simeq 28$

cm^{-1}. That is, a 12% decrease of $\bar{\omega}_v$ is indicated. Below 169 K the temperature dependence of the NQR frequency is complicated by the lattice distortion and no detailed analysis has been attempted.

The ^{79}Br spin lattice relaxation time (T_1) data for K_2PtBr_6 are shown in Fig. 5. The data exhibit a distinct minimum at 169 K. Below 169 K the two symbols correspond to the relaxation times for the two types of ^{79}Br nuclei. It is interesting to note that the T_1 data provide no evidence for the lower temperature phase transitions. Measurements of the ratio of relaxation times for the ^{79}Br and ^{81}Br nuclei indicate that a nuclear quadrupole relaxation mechanism is responsible for T_1. The relaxation time for an X nucleus in an R_2MX_6 compound has been shown to be dominated by the anharmonic Raman process and in the cubic phase is given by (5)

$$\frac{1}{T_1} = \frac{9\pi}{8\hbar}\left(\frac{eQk_BT}{m_xRN}\right)^2 \sum_{\lambda_1\lambda_2} |\gamma(\lambda_1\bar{\lambda}_2)|^2 \left| \sum_{\substack{\alpha=x,y \\ \lambda_3}} f_\alpha^{+1}(M|X)\frac{e_\alpha(X|\lambda_3)}{\omega_{\lambda_3}^2}\right|^2$$
$$x\,\delta(\varepsilon_{\lambda_2} - \varepsilon_{\lambda_1} - \varepsilon_Q)\,\Delta(\mathbf{k}_1 - \mathbf{k}_2 - \mathbf{k}_3)$$

where eQ is the nuclear quadrupole moment, $\lambda = (\mathbf{k}j)$ and $\varepsilon_\lambda = \hbar\omega_\lambda$. On the basis of a point charge, nearest neighbor approximation $f_\alpha^{+1}(M|X) = 3se/\sqrt{6}\ R^4$ with s a factor to take account of covalency and antishielding. The λ_3's are taken to be rotary-lattice modes; other bond bending modes are neglected since they are considerably higher in energy. The quantity $\gamma(\lambda_1, \bar{\lambda}_2)$ is a generalized Grüneisen parameter. This expression is obtained using a perturbation theory approach (6) and is therefore not expected to apply within the critical region associated with the phase transition. Since the size of the critical region is not known for K_2PtBr_6 it is not known where this expression will breakdown but it is reasonable to expect that it will hold to within a few degrees of T_c. Neglecting the $\mathbf{k}$ dependence of the eigenvectors and assuming that ω_{λ_i} and $\gamma(\lambda_1, \bar{\lambda}_2)$ are independent of $\mathbf{k}$ it follows that

$$\frac{1}{T_1} = \frac{243\pi}{32}\left(\frac{e^2sQk_BT}{\hbar m_{Br}R^5}\right)^2 \frac{\gamma^2}{\bar{\omega}_{T_1}^5}$$

with γ the macroscopic Grüneisen parameter for the crystal. The Brillouin zone averaged rotary mode frequency $\bar{\omega}_{T_1}$ is defined as

$$\bar{\omega}_{T_1} = \left[\frac{V_c}{9\pi\gamma^2}\sum_{jj'}\int_0^\pi\int_0^{k_{max}} \frac{\gamma^2(\mathbf{k}j, \mathbf{k}'j')\,k^4\,dk\cos\theta\,d\theta}{\omega_{rot}^4(2k\sin\theta/2)\left|\frac{\partial\omega_j(k)}{\partial k}\right|}\right]^{-1/5}$$

where θ is the angle between $\mathbf{k}$ and $\mathbf{k}'$. The temperature dependence of $\bar{\omega}_{T_1}$ as obtained from the T_1 data is shown in Fig. 6. At 300 K $\bar{\omega}_{T_1} \simeq 27\ cm^{-1}$, whereas at 169 K $\bar{\omega}_{T_1} \simeq 16$ cm^{-1}. That is, a 40% decrease of $\bar{\omega}_{T_1}$ is indicated. The difference in the amount of softening experienced by $\bar{\omega}_v$ and $\bar{\omega}_{T_1}$ is in agreement with the theoretical conclusion that the spin lattice relaxation is dominated by the anharmonic Raman process and not by the first-order Raman process.

Below 169 K there are two different T_1's, namely $T_{1_{x,y}}$ and T_{1_z} associated with the corresponding resonances whose frequencies are given in Fig. 3. It is observed that $T_{1_{x,y}} \simeq 2T_{1_z}$. Because the field gradients at the two inequivalent Br sites do not differ by

more than 1%, the difference between $T_{1_{x,y}}$ and T_{1_z} must be dynamical in origin. This difference must be associated with a difference in the respective librational potential wells such that $(\bar{\omega}_{T_1})_z$ is larger than $(\bar{\omega}_{T_1})_{x,y}$ (*7*).

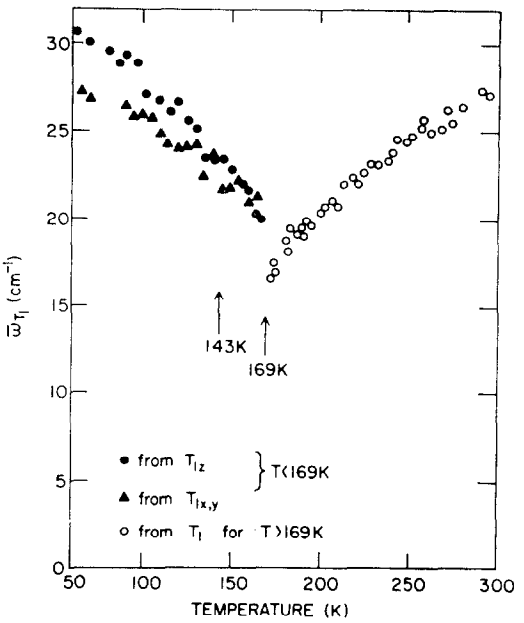

FIG. 6. Temperature dependence of the average rotary-lattice mode frequency $\bar{\omega}_{T_1}$.

3. CHLORINE NQR IN K_2ReCl_6 (*8–11*)

The ^{35}Cl NQR frequency data obtained from a powder sample of K_2ReCl_6 over the temperature range from 70 to 360 K are shown in Fig. 7. Above 111 K a single resonance line, as characteristic of the cubic antifluorite structure, is observed. The data clearly show the presence of three structural phase transitions at 76, 103, and 111 K; however, only the transition at 111 K will be considered in detail. This transition is believed to be of the tilting variety and induced by the softening of a rotary-lattice mode. The specific heat data (*12*) exhibit a small anomaly at 111 K and therefore indicate that the phase transition is purely displacive in nature. X-ray scattering data (*13*) show that the unit cell size is the same both above and below 111 K and therefore show that a zone center phonon is involved in the phase transition. A nuclear magnetic resonance experiment (*14*) carried out on a single crystal of K_2ReCl_6 has provided evidence that the $ReCl_6$ octahedra do indeed reorient in the distorted phase and that the angle of rotation of the octahedra increases from 0° to 3° as the temperature is lowered from 111 to 103 K. A point charge calculation (*2*) of the lattice contribution to the electric field gradient at a chlorine site shows that the observed frequency splitting between the two NQR lines is consistent with this conclusion.

A rigid-ion model for K_2ReCl_6 at 300 K has been constructed (*13*). In the model the ions are assumed to be nonpolarizable and to interact pairwise via central forces which can be separated into short-range interactions and long-range Coulomb interactions.

With the exception of the Re–K pair, all atoms within the unit cell are assumed to interact with one another and with symmetry related atoms. In addition, octahedron–octahedron interactions are included by allowing a chlorine atom of a given octahedron to interact with the two nearest chlorine atoms on adjacent octahedra. In total, seven types of short-range interactions are included. Each such interaction is described by both a parallel and a perpendicular force constant; these are related to the first and second derivatives of the potential with respect to the atomic separation. The Coulomb interactions are characterized by three effective charges–one for each type of ion. The number of independent parameters in the model is reduced by three by the requirements for charge neutrality and static equilibrium. As input data for determining the 14 independent parameters there are available 22 phonon energies, some at the center and others at the edge of the Brillouin zone. Zone-boundary energies were deduced from conventional spectroscopic measurements taken below 103 K where the unit cell is four times as large as in the cubic phase. Once the parameters of the model had been obtained, dispersion curves for all of the phonon branches were calculated. The predicted rotary-lattice mode has a zone-center frequency of 46 cm^{-1} and exhibits considerable dispersion. It is as a result of the dispersion of the rotary-lattice mode that $\bar{\omega}_v$ and $\bar{\omega}_{T_1}$ as deduced from the K_2PtBr_6 data are different. The zone-center frequency Γ^{15+} depends on the force constants of the model according to

$$\omega^2_{\Gamma^{15+}} = \frac{2}{m_{Cl}}(A_1 - B_1 + 2A_2) + \text{Coulomb terms},$$

where A_1 and B_1 are the parallel and perpendicular force constants associated with the K–Cl interaction and A_2 is the parallel force constant associated with the next nearest neighbor octahedron–octahedron interaction. By the variation of A_1 and B_1 only, it is possible to drive the Γ^{15+} mode frequency from 46 cm^{-1} to zero while not severely affecting the frequencies of the other modes. That is, the rigid-ion model is consistent with the geometrical picture of a tilting-type phase transition.

The rigid-ion model was further exploited (*15*) to yield the eigenvectors at a series of points in the Brillouin zone. The result of this exercise was to demonstrate a marked variation in the rotary character of various modes with **k**-vector. Calculations of mean-squared angular amplitudes revealed that the change in the rotary character of the eigenvectors across the Brillouin zone has an important influence on the thermal averaging of the electric field gradient and therefore on the NQR frequency. In particular, the rotary-lattice mode contributes only 35% of the total NQR frequency shift at 300 K from the static lattice value rather than the 72% predicted on the basis of zone-center eigenvectors. Since in K_2PtBr_6 the rotary-lattice mode lies considerably lower in frequency, it will mix less with the translatory-lattice modes and will retain more of its rotary character throughout the Brillouin zone. Nonetheless, the results obtained for K_2PtBr_6 must be considered to have qualitative rather than quantitative significance.

As shown in Fig. 7 the ^{35}Cl NQR frequency above 111 K increases as the temperature increases; above 275 K, $(\partial\nu/\partial T)_P = 0.06$ kHz K^{-1}. Such anomalous behavior has been attributed to the presence in the Re–Cl bond of a weak π character in addition to the strong σ character. Fig. 8 shows the ^{35}Cl NQR frequency data as a function of applied hydrostatic pressure at 277 K. From these and similar data $(\partial\nu/\partial P)_T = -0.011$ kHz kg^{-1} cm^2 for $277 < T < 350$ K. But, in this temperature range, the ratio α/β of the

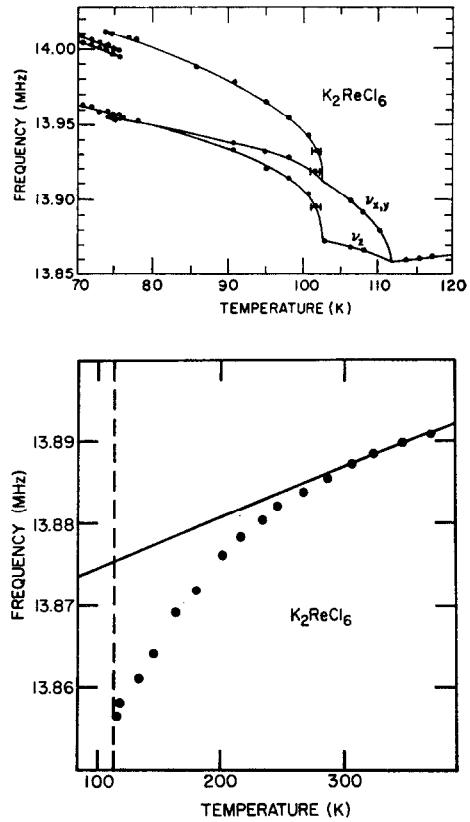

FIG. 7. Temperature dependence of the ^{35}Cl NQR frequency in K_2ReCl_6.

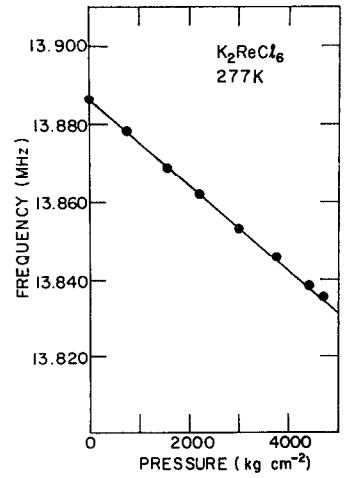

FIG. 8. Pressure variation of the ^{35}Cl NQR frequency in K_2ReCl_6.

thermal expansion coefficient α to the isothermal compressibility β is $\simeq 39$ kg cm^{-2} K^{-1}, so that

$$\frac{\alpha}{\beta}\left|\left(\frac{\partial v}{\partial P}\right)_T\right| = 0.44 \gg \left(\frac{\partial v}{\partial T}\right)_P = 0.06.$$

That is, specific volume effects dominate the temperature variation of the NQR frequency in K_2ReCl_6. In this case

$$\nu(T) = \nu_0(V, T)\,[1 - \tfrac{3}{2}\xi\langle\theta_x^2(T)\rangle - \tfrac{3}{2}\xi\langle\theta_y^2(T)\rangle],$$

where $\nu_0\,(V, T)$ is the static lattice resonance frequency for volume V, temperature T, and ξ is a constant which relates to the amount of π-bonding. The appearance of the factor ξ assumes that bond bending modes cause a destruction of π-bonding (*16*). If this does not occur (*17*) then $\xi = 1$. Assuming that $\nu_0(V, T)$ is a linear function of temperature it follows that to first order

$$\nu(T) = \nu_0^0(1 + \chi T) - \tfrac{3}{2}\xi\nu_0^0[\langle\theta_x^2(T)\rangle + \langle\theta_y^2(T)\rangle]$$

with

$$\chi\nu_0^0 = -\frac{\alpha}{\beta}\left(\frac{\partial v}{\partial P}\right)_T.$$

Taking $\nu_0^0 = 13.868$ MHz, $\chi = 3.19 \times 10^{-5}$ K^{-1}. With the aid of this expression the temperature dependence of $\xi\langle\theta_\alpha^2(T)\rangle$ can be extracted from the data. The rigid-ion model computer program may be used to determine the temperature dependence of the zone center rotary-lattice mode frequency. To do this ξ is chosen as 0.772 which makes the calculated value of $\langle\theta_\alpha^2(T)\rangle$ agree with the experimental results at 300 K.

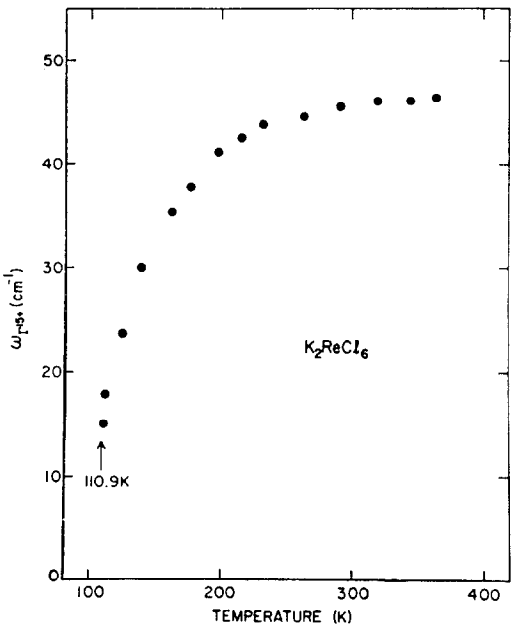

FIG. 9. Temperature dependence of the Γ^{15} rotary-lattice mode in K_2ReCl_6.

The K–Cl force constants are then varied in order that the model reproduce the values of $\langle\theta_\alpha^2(T)\rangle$ deduced from the NQR data at all other temperatures. The result of this fitting procedure is shown in Fig. 9. The zone-center frequency decreases from 46 cm^{-1} at 300 K to 15 cm^{-1} at 111 K. It follows from the dispersion curves and eigenvectors for the model that $\bar{\omega}_v$ decreases from 64 cm^{-1} to 57 cm^{-1} over the same temperature range, a softening of 11 %. This result is very similar to that deduced from the K_2PtBr_6 data.

The chlorine nuclear spin-lattice relaxation process in K_2ReCl_6 is dominated by the hyperfine interaction between the chlorine nucleus and the unpaired electron spin of the $ReCl_6$ complex ion. Therefore, the T_1 data in K_2ReCl_6 contain no information relating to the structural phase transitions.

4. CHLORINE NQR IN $CsPbCl_3$ (*11, 18, 19*)

The ^{35}Cl NQR frequency data obtained from a powder sample of $CsPbCl_3$ over the temperature range from 100 to 360 K are shown in Fig. 10. Structural phase transitions are indicated at 310, 315, and 320 K. Neutron scattering experiments (*20*) have shown

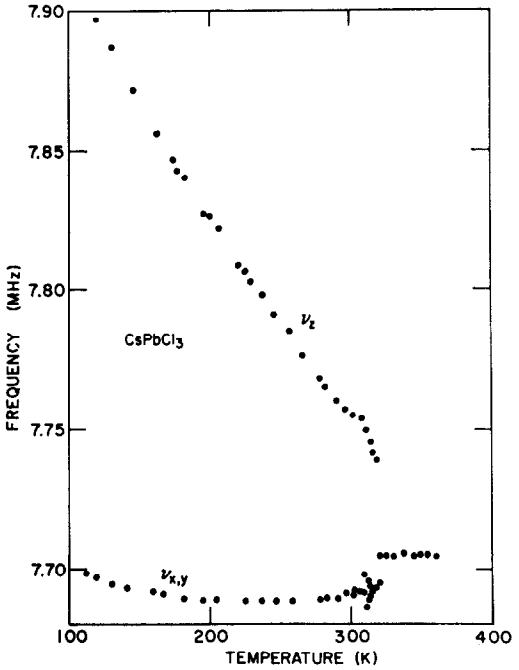

FIG. 10. Temperature dependence of the ^{35}Cl NQR frequency in $CsPbCl_3$.

that all three transitions are of the tilting type and are associated with the softening of the R^{25-} and M^{3-} librational modes of the $PbCl_6$ octahedra. The NQR frequency data are consistent with the neutron structural determinations shown in Fig. 11. In phase I ($T > 320$ K), all Cl ions are at equivalent sites characteristic of the cubic perovskite structure. A single NQR line is observed. In phase II ($315 < T < 320$ K), Cl-β ions and

Cl-γ ions are crystallographically equivalent but inequivalent to Cl-α ions. Two NQR lines with a 2 : 1 intensity ratio are observed. In phase III ($310 < T < 315$ K), Cl-β ions and Cl-γ ions become inequivalent since the equilibrium positions of the $PbCl_6$ octahedra have been rotated about an axis perpendicular to the tetragonal axis of phase II. The Cl-β ions have been rotated out of the plane perpendicular to the tetragonal axis; the Cl-γ ions remain in the plane. Therefore, in phase III the Cl-β ions and Cl-γ ions give rise to different resonance lines. In phase IV ($T < 310$ K), the $PbCl_6$ octahedra

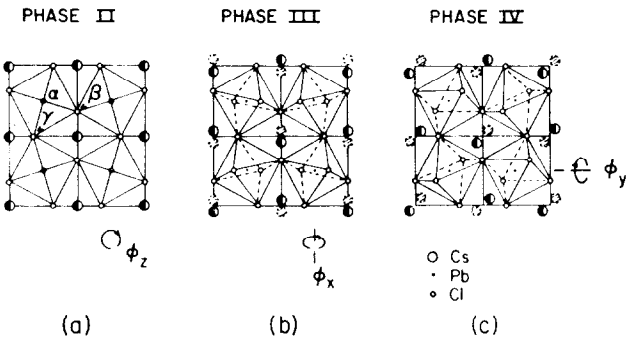

FIG. 11. Illustration of the ionic positions in the distorted phases of $CsPbCl_3$. (a) Phase II, $315 < T < 320$ K, (b) Phase III, $310 < T < 315$ K, (c) Phase IV, $T < 310$ K.

rotate about an axis perpendicular to the other two axes of rotation. As a result the ionic arrangements around the Cl-β ions and Cl-γ ions are similar even though these sites are not crystallographically equivalent. The separate resonances for the Cl-β ions and Cl-γ ions of phase III are observed to merge in phase IV suggesting a frequency splitting of less than 1 kHz.

The general magnitude of the ^{35}Cl NQR frequency in $CsPbCl_3$ can be accounted for on the basis of a point charge model for the calculation of the electric field gradient with each ion having its formal charge. The major contribution (>75%) to the field gradient comes from the two nearest Pb ions. Therefore, it is the modulation of this contribution by the Pb-Cl-Pb bond bending motions which will dominate the thermal averaging of the electric field gradient.

A rigid-ion model of $CsPbCl_3$ has been constructed considering Pb-Cl, Cl-Cl, and Cl-Cs short range interactions and taking the ions to have their formal charges for the calculation of the long range Coulomb interactions. The five independent parameters were obtained by fitting to elastic-constant data (*21*) and acoustic-mode frequency data (*20*). The characteristic frequencies of the T^{2-} phonon branch along the $(1, 1, \xi)$ direction, which is compatible with the M^{3-} and R^{25-} modes for $\xi = 0$ and $\xi = 1$, respectively, are given by

$$\omega^2(T^{2-}) = \frac{1}{m_{Cl}}(A_1 - 3B_1) + \frac{e^2 Z_{Cl}^2}{a^3} C(\xi),$$

where A_1 and B_1 are the parallel and perpendicular Cl-Cs force constants, m_{Cl} and eZ_{Cl} are the mass and charge of the chlorine ion and a is the lattice constant. The electrostatic parameter $C(\xi)$ shows little ξ dependence along the $(1, 1, \xi)$ direction which implies

nearly flat dispersion for the T^{2-} branch. The M^{3-} and R^{25-} rotary-lattice modes are therefore expected to be close in energy. The model shows that they are also very low in energy so that the thermal averaging of the electric field gradient will be almost entirely due to the rotary-lattice modes. Finally, any softening of the M^{3-} and R^{25-} rotary-lattice modes is most likely to be associated with a weakening Cl-Cs interaction as expected for a tilting-type phase transition.

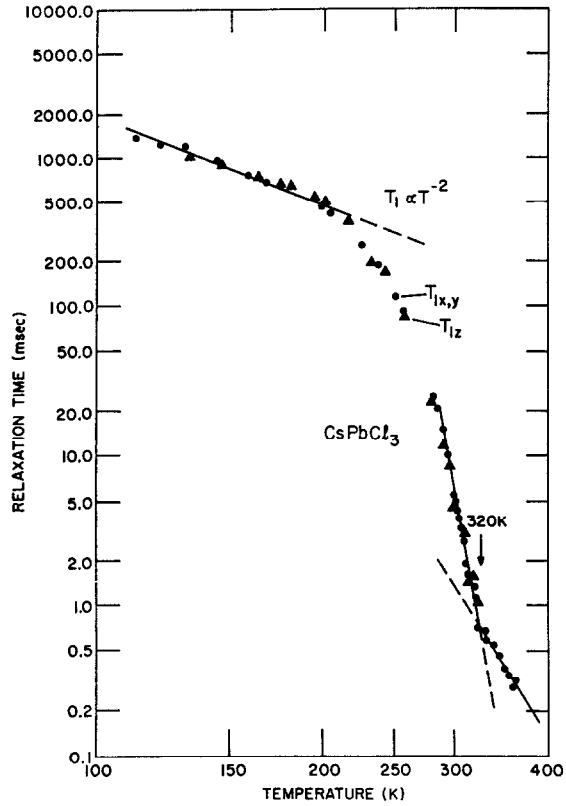

FIG. 12. Temperature dependence of the ^{35}Cl spin-lattice relaxation time in $CsPbCl_3$.

No further analysis of the NQR data is reasonable without information on specific volume effects. The fact that the NQR frequency in the cubic phase is almost temperature independent suggests that such effects are important in $CsPbCl_3$.

The ^{35}Cl spin-lattice relaxation data in $CsPbCl_3$ are shown in Fig. 12. Below 200 K the relaxation time varies as T^{-2} as expected for an harmonic and dynamically stable lattice. Above 200 K the relaxation time begins to decrease in an anomalous fashion suggesting the onset of an instability in the lattice. In particular, these data reflect a substantial softening of the rotary-lattice modes which are associated with the structural phase transitions occurring just above 300 K. The T_1 data exhibit a discontinuity at 320 K, the temperature of the cubic to tetragonal phase transition. Note, however, that no T_1 minimum occurs, in contrast to the case of K_2PtBr_6. It is believed that the behavior of $CsPbCl_3$ is anomalous because of its anharmonic character above 300 K.

Raman scattering experiments (*22*) in the distorted phases of $CsPbCl_3$ have shown that the soft modes become heavily overdamped above 300 K. Neutron scattering experiments (*2*) have shown that the rotary-lattice modes are also heavily damped up to 350 K and that the Debye-Waller factor for the chlorine ions is extraordinarily large in the cubic phase. It is therefore likely that the $PbCl_6$ octahedra will undergo hindered rotational motions thereby providing a very efficient second relaxation mechanism for the chlorine nuclear spins. The contribution to the nuclear spin relaxation rate from such a mechanism is of the form (*23*)

$$T_1^{-1} = C\exp(-V_0/kT),$$

where C is a constant and V_0 is the height of the potential barrier to rotation. It follows that the measured T_1 will continue to decrease as the temperature increases above 320 K.

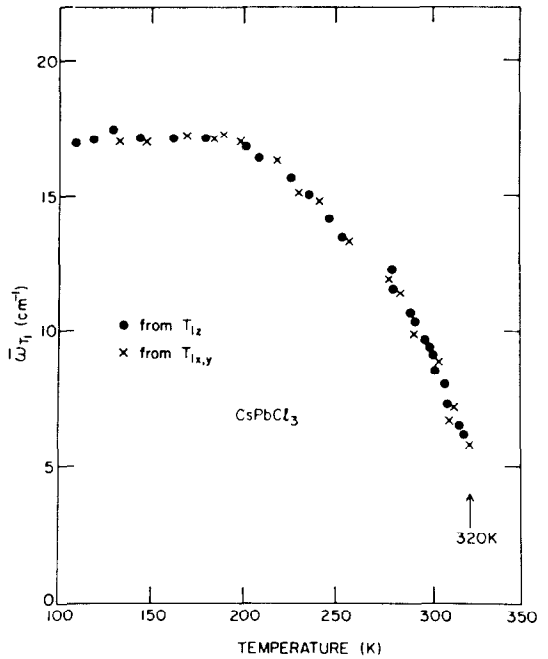

FIG. 13. Temperature dependence of the average rotary-lattice mode frequency $\bar{\omega}_{T_1}$.

Below 300 K the lattice anharmonicity is small and the perturbation treatment of relaxation referred to in Section 2 (*5*) is again applicable. In this case, however, the expression for $\bar{\omega}_{T_1}$ is not as simple as it was for K_2PtBr_6 where it could be reasonably assumed that $e_\alpha(X|\mathbf{k}j_{\text{rot}})$ was independent of $\mathbf{k}$. From the dispersion curves for $CsPbCl_3$ it is apparent that the rotary-lattice modes at the zone boundary become acoustic modes or optic modes at the zone center and therefore that the nature of the mode eigenvectors changes significantly across the Brillouin zone. The acoustic modes near the zone center involve nearly uniform translation of the atoms in the unit cell and therefore do not contribute to $\bar{\omega}_{T_1}$; the optic modes are much higher in energy than the

rotary modes and do not contribute significantly to $\bar{\omega}_{T_1}$. The expression for $\bar{\omega}_{T_1}$ primarily reflects the behavior of the soft zone boundary rotary-lattice modes. Figure 13 shows the temperature dependence of $\bar{\omega}_{T_1}$. As the temperature increases from 200 to 300 K, $\bar{\omega}_{T_1}$ decreases from 17 cm^{-1} to 6 cm^{-1}. The softening by 66% is considerably larger than that observed in K_2PtBr_6 and reflects the effect on $\bar{\omega}_{T_1}$ of the softening of a zone-boundary mode in the one case and a zone-center mode in the other.

There are two additional observations concerning the T_1 data in $CsPbCl_3$. First there is a thermal hysteresis effect associated with the measurements in the vicinity of the 320 K phase transition. Similar hysteresis effects have also been noted in electrical conductivity experiments (*24*) on $CsPbCl_3$. Second, for the data between 290 and 360 K the return of the spin system to equilibrium following a saturating pulse is nonexponential. These phenomena are not well understood.

5. CHLORINE NQR IN K_2OsCl_6 (*25, 26*)

Measurements of the ^{35}Cl NQR frequency in K_2OsCl_6 reveal the presence of a structural phase transition near 45 K. Specific heat measurements (*27*) show that the transition is purely displacive in nature. An analysis of NQR frequency data in the cubic phase indicates that the rotary-lattice mode softens to drive the transition. Both thermal expansion data (*28*) and NQR free induction decay measurements indicate that the region of critical fluctuations extends about 10 K above T_c. The compound K_2OsCl_6 is therefore a convenient antifluorite for the study of critical dynamics.

The chlorine spin-lattice relaxation data are particularly interesting. For a powder sample the recovery of the nuclear magnetization below 120 K following a saturating pulse cannot be described by a single exponential; above 120 K the recovery of the magnetization is exponential. The data below 120 K were analyzed using a two exponential model and the temperature dependence of the two relaxation times deduced (T_1^l and T_1^s) are shown in Fig. 14. The fractional number of nuclei that contribute to T_1^s increases dramatically as T approaches T_c. This is shown in Fig. 15. For a single crystal of K_2OsCl_6 the recovery of the magnetization was exponential at all temperatures. The temperature dependence of T_1 for the crystal was very nearly that of T_1^l in the powder sample. The powder sample was heated to 10 K below its decomposition temperature and held there for 1 week. The only effect on the NQR data was to increase the length of the free induction decay signals by 10 to 20%. The average size of the crystallites in the powder sample was reduced by grinding. None of the NQR data was altered as a result of this process. A number of conclusions can be drawn: (1) The observation of two relaxation times for an essentially two-level system requires two distinguishable sets of nuclei; (2) The rapid growth of the signal corresponding to T_1^s as T approaches T_c suggests that the presence of T_1^s must be related to the occurrence of the structural phase transition; (3) The failure to observe a T_1^s component in a single crystal grown from solution implies that impurities are essential for the appearance of the second component. The T_1^l component in the powder and T_1 in the single crystal are associated with the usual thermal fluctuations of the local electric field gradients and the temperature dependence of T_1^l reflects the condensation of the rotary-lattice mode phonons which are responsible for the phase transition. This interpretation was confirmed by measuring the isotopic ratio of T_1^l values. The T_1^s component is believed to be associated with the presence of regions of correlated fluctuations (dynamic

clusters) which anticipate the symmetry of the low temperature phase. In the region of a cluster the symmetry in the vicinity of a particular nucleus can change abruptly. Such changes in symmetry could give rise to a nonresonant relaxation mechanism with an

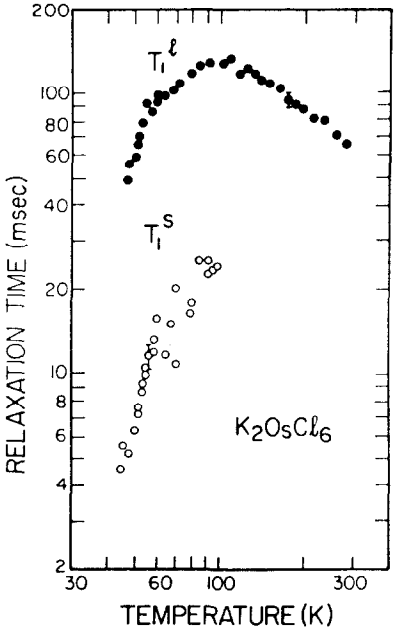

FIG. 14. Temperature dependence of the two ^{35}Cl spin-lattice relaxation times T_1^l and T_1^s observed in a powder sample of K_2OsCl_6.

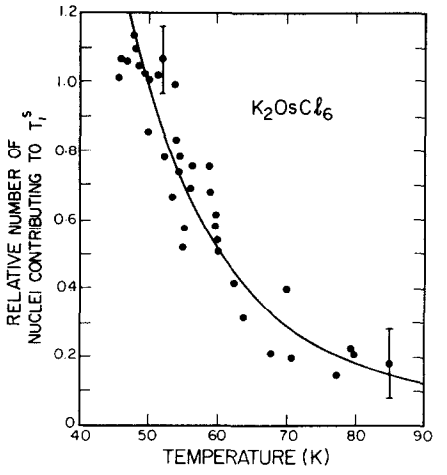

FIG. 15. Temperature dependence of the ratio of the relative number of nuclei contributing to the T_1^s component as compared to the T_1^l component.

efficiency which increases as T approaches T_c. Indeed, the isotopic ratio of T_1^s values is unity and the magnitude of T_1^s decreases with decreasing temperature. If impurities act as nucleation sites for cluster formation, nuclei near impurities will be distinguishable

from nuclei far from impurities. If two physically distinct Cl sites occur in the powder above T_c but not in the single crystal, the NQR frequency data should reflect this difference and indeed they do (*26*). As T approaches T_c the coherence length of the correlated fluctuations will increase so that the number of nuclei contributing to the T_1^S component will also increase. That is, all of the evidence points to the existence of dynamics clusters in the cubic phase of a powder sample of K_2OsCl_6 near T_c.

6. SUMMARY

The bromine NQR frequency and spin-lattice relaxation measurements in K_2PtBr_6 are analyzed on the assumption that the cubic to tetragonal structural phase transition is of the tilting variety and results from the condensation of the Γ^{15+} zone-center rotary-lattice mode phonon. Two averages $\bar{\omega}_\nu$ and $\bar{\omega}_{T_1}$ of the rotary-lattice mode frequency over the Brillouin zone are defined. The data indicate that $\bar{\omega}_{T_1}$ softens more than $\bar{\omega}_\nu$ in agreement with the theoretical conclusion that T_1 is dominated by the anharmonic Raman process.

A rigid-ion model calculation for K_2ReCl_6 shows that the high temperature phase transition could be brought about by a weakening K-Cl interaction corresponding to a softening of the Γ^{15+} rotary-lattice mode. The calculation also illustrates the importance of changes in the rotary character of eigenvectors across the Brillouin zone to the thermal averaging of the electric field gradient. Specific volume effects dominate the temperature variation of the NQR frequency. With the help of the rigid-ion model, the data are analyzed to obtain the temperature dependence of the frequency of the Γ^{15+} mode and of $\bar{\omega}_\nu$. The result for $\bar{\omega}_\nu$ in K_2ReCl_6 is very similar to that for K_2PtBr_6.

The occurrence of tilting type phase transitions in $CsPbCl_3$ have been confirmed by neutron scattering experiments. The NQR frequency spectrum is consistent with the neutron structural determinations. A rigid-ion model calculation shows that the softening of the M^{3-} and R^{25-} rotary-lattice modes may be associated with a weakening Cl-Cs interaction. The spin-lattice relaxation data reflect the condensation of the rotary-lattice mode phonons as expected but also show the effect of the high degree of lattice anharmonicity above 300 K.

Spin-lattice relaxation time data taken in a powder sample of K_2OsCl_6 differ markedly from those taken in a single crystal. The difference is attributed to the formation of dynamic clusters near to impurity sites in the powder sample. The symmetry within these clusters is that of the distorted phase even though the temperature of the sample is higher than the transition temperature.

ACKNOWLEDGMENTS

The majority of the University of Toronto results presented were obtained as part of the Ph.D. programs of H.M. van Driel and C. A. Martin. I thank them for their dedication and hard work.

REFERENCES

1. H. M. VAN DRIEL, M. WISZNIEWSKA, B. M. MOORES, AND R. L. ARMSTRONG, *Phys. Rev. B* **6,** 1596 (1972).
2. M. WISZNIEWSKA AND R. L. ARMSTRONG, *Can. J. Phys.* **51,** 781 (1973).
3. T. KUSHIDA, G. B. BENEDEK, AND N. BLOEMBERGEN, *Phys. Rev.* **104,** 1364 (1956).
4. R. L. ARMSTRONG, G. L. BAKER, AND K. R. JEFFREY, *Phys. Rev. B* **1,** 2847 (1970).
5. H. M. VAN DRIEL AND R. L. ARMSTRONG, *Can. J. Phys.*, **53,** 1141 (1975).

6. J. VAN KRANENDONK AND M. B. WALKER, *Can. J. Phys.* **46,** 2441 (1968).
7. H. M. VAN DRIEL, Ph.D. Thesis, University of Toronto, 1974.
8. G. P. O'LEARY, *Phys. Rev. Lett.* **23,** 782 (1969).
9. R. L. ARMSTRONG, G. L. BAKER, AND H. M. VAN DRIEL, *Phys. Rev. B* **3,** 3072 (1971).
10. G. P. O'LEARY, *Phys. Rev. B* **3,** 3075 (1971).
11. H. M. VAN DRIEL, R. L. ARMSTRONG, AND M. M. MCENNAN, *Phys. Rev., B* **12,** 488 (1975).
12. R. H. BUSEY, H. H. DEARMAN, AND R. B. BEVAN, JR., *J. Phys. Chem.* **66,** 82 (1962).
13. G. P. O'LEARY AND R. G. WHEELER, *Phys. Rev. B* **1,** 4409 (1970).
14. A. G. BROWN, R. L. ARMSTRONG, AND K. R. JEFFREY, *Phys. Rev. B* **8,** 121 (1973).
15. H. M. VAN DRIEL, M. M. MCENNAN, AND R. L. ARMSTRONG, *J. Mag. Resonance,* **18,** 485 (1975).
16. T. E. HAAS AND E. P. MARRAM, *J. Chem. Phys.* **43,** 3985 (1965).
17. T. L. BROWN AND L. G. KENT, *J. Phys. Chem.* **74,** 3572 (1970).
18. N. TOVBORG-JENSEN, *J. Chem. Phys.* **50,** 559 (1969).
19. H. M. VAN DRIEL AND R. L. ARMSTRONG, *Phys. Rev., B* **12,** 839 (1975).
20. Y. FUJII, S. HOSHINO, Y. YAMADA, AND G. SHIRANE, *Phys. Rev. B* **9,** 4549 (1974).
21. K. S. ALEKSANDROV, A. I. KRUPNYI, V. I. ZINENKO, AND B. V. BEZNOSIKOV, *Sov. Phys.-Cryst.* **17,** 515 (1972).
22. S. HIROTSU, *J. Phys. Soc. Jap.* **28S,** 185 (1970); **31,** 552 (1971).
23. K. R. JEFFREY AND R. L. ARMSTRONG, *Phys. Rev.* **174,** 359 (1968).
24. O. BUSMUNDRUD AND J. FEDER, *Solid State Commun.* **9,** 1575 (1971).
25. R. L. ARMSTRONG AND C. A. MARTIN, *Phys. Rev. Lett.*, **35,** 294 (1975).
26. C. A. MARTIN AND R. L. ARMSTRONG, to appear.
27. V. NOVOTNY, C. A. MARTIN, P. P. M. MEINCKE, AND R. L. ARMSTRONG, to appear.
28. H. M. WILLEMSON, C. A. MARTIN, P. P. M. MEINCKE, AND R. L. ARMSTRONG, to appear.